Chapter 5. Redox Properties and Electronic Structure of Iron and Cobalt Supported Dinitrogen Complexes

Portions of the following work were completed in collaboration with Dr. Mark P. Mehn.

Abstract

The [$PhBP^{iPr}_3$] ligand can support a single iron or cobalt center in a pseudo-tetrahedral environment in which dinitrogen is bound in the fourth coordination site. While the zero-valent metal-dinitrogen complexes have the general formula [([$PhBP^{iPr}_3$]M(μ-N_2))$_2$[Mg^{2+}] (M = Fe, Co, [$PhBP^{iPr}_3$] = [$PhB(CH_2P^iPr_2)_3]^-$), bridging structures are also be obtained as neutral [M^I]—N_2—[M^I] complexes, or as their reduced anions [M^I]—N_2—[M^0] ([M] = [$PhBP^{iPr}_3$]Fe, [$PhBP^{iPr}_3$]Co). The latter mixed-valence compounds exhibit delocalization of the anionic charge, as evidenced by their crystallographic behavior and IR spectra. The nature of the structural distortions observed in both [M](μ-N_2)]$_2$[Mg^{2+}] and [M^n]—N_2—[M^n] complexes are described. Magnetic characterization of the neutral and mixed-valence dimeric complexes reveal the complexes remain ferromagnetically coupled over all temperatures investigated. The molecular bonding orbital interactions are described for both the monomeric and dimeric dinitrogen complexes with the spin-state descriptions provided for the complexes presented herein.

5.1. Introduction

The coordination modes for dinitrogen on transition metal complexes can be widely varied.[1] When the metal has populated orbitals of appropriate symmetry to mix with the π* orbitals on N_2, back π-donation from the metal to the N_2 can occur as well. As this M→N_2 π* bonding increases, the N_2 ligand becomes strongly activated and may be best described as formally reduced to diazenido (N_2^-) or hydrazido (N_2^{2-}) functionalities. Metal complexes featuring strongly activated N_2 ligands can exhibit N—N bond elongation and can exhibit nucleophilic character of the bound N_2 as gauged by its reactivity with electrophilic reagents (e.g., H_3C^+, H^+).[2]

The early and mid-transition metals have demonstrated the capacity to activate N_2 in a large number of cases.[3] Mid-valent metal complexes will often coordinate and reduce N_2 to formally oxidize the metal center(s). One extreme example of this reaction type where N_2 is strongly activated is the Mo trisanilide complex reported by Cummins.[4] In this case, the N_2 ligand is activated by two three-coordinate Mo^{III} centers to cleave the N—N bond through an intermediate hydrazido ligand, thermodyanimically driven to form two strong Mo—N triple bonds (Scheme 5.1).

Scheme 5.1

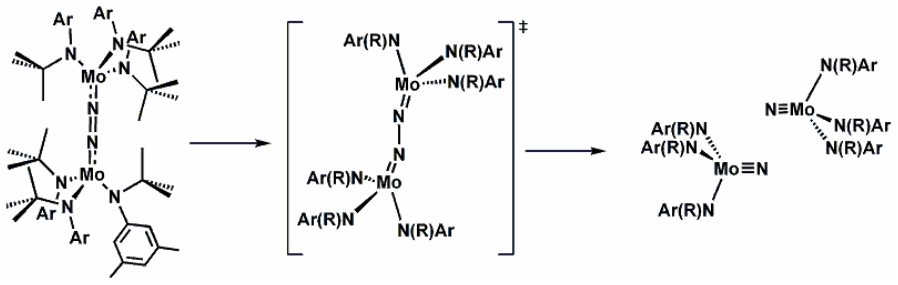

Late transition metal N_2 complexes are more typical of weakly-activated N_2 complexation.[5] In many of these cases, the N—N bond is not substantially elongated beyond that of free dinitrogen.[6] However, Holland's recent report where dinitrogen is reduced in a stepwise fashion in a diiron complex suggests that late transition metals, specifically iron, can be adept at binding and weakening of N_2 when the metal coordination numbers are minimized (Scheme 5.2).[7]

Scheme 5.2

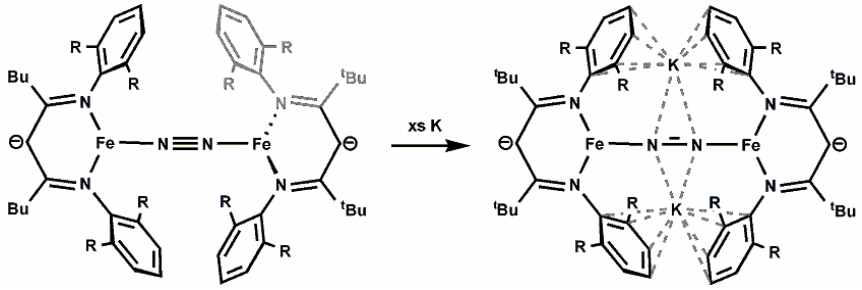

Recent work by our group has shown that trigonally coordinated iron and cobalt subunits of the form "[PhBP$^{i\text{Pr}}_3$]M" ([PhBP$^{i\text{Pr}}_3$] = [PhB($CH_2P^iPr_2$)$_3$]$^-$) accommodate both strongly π-accepting (e.g., N_2) and strongly π-donating ligands (e.g., NR^{2-}, N^{3-}) at the fourth site along their pseudo threefold axis.[8] Chemical reduction of Fe or Co [PhBP$^{i\text{Pr}}_3$]M—X precursors provided facile entry into dinitrogen coordination chemistry where examples of both strongly activated N_2 ligands (e.g., diazenido in [PhBP$^{i\text{Pr}}_3$]M(N_2)$^-$) and weakly activated N_2 ligands can be obtained (e.g., [PhBP$^{i\text{Pr}}_3$]M—N_2—M[PhBP$^{i\text{Pr}}_3$]). Herein, we discuss the structural characteristics of these N_2 complexes and describe their electronic ground states based on their magnetic characterization.

5.2. Results and Discussion

Scheme 5.3

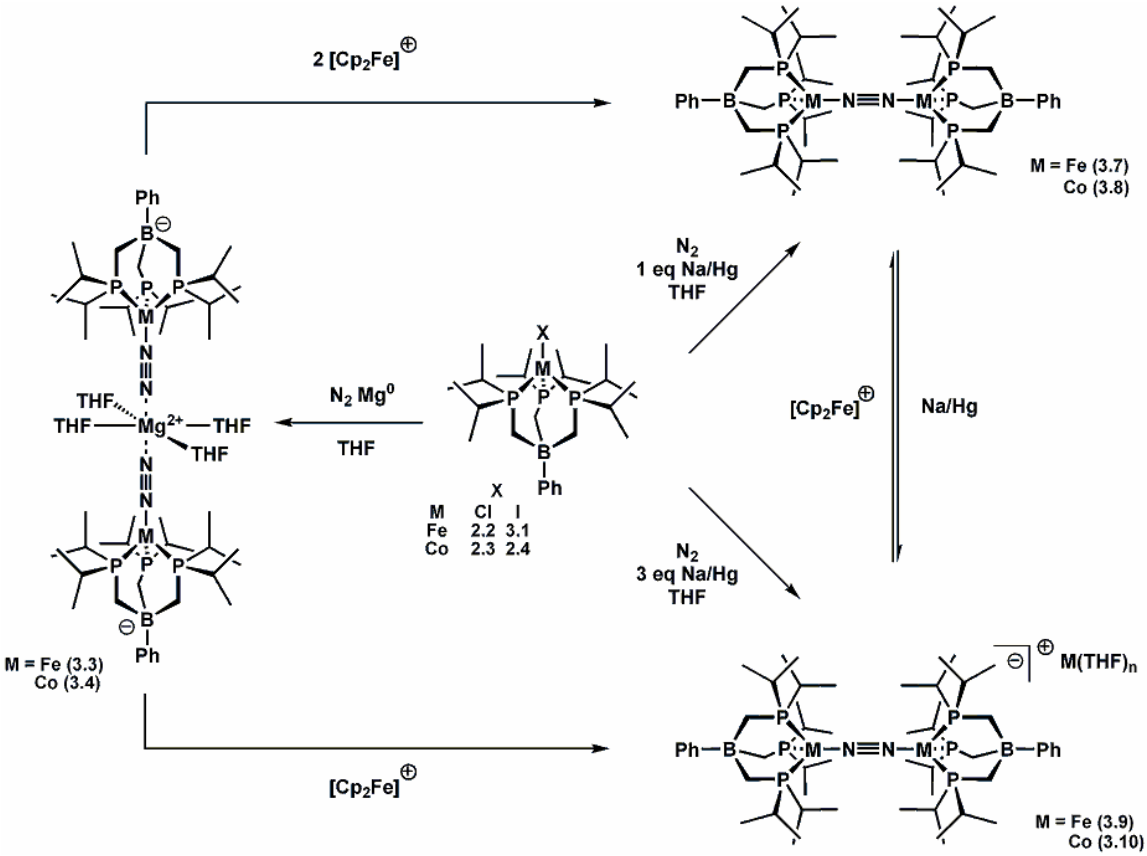

5.2.1. Synthesis of Dinitrogen Complexes. As previously reported,[8a] the synthesis of M—N_2 complexes begins with the divalent precursors [PhBP$^{i\text{Pr}}_3$]M—X (M = Fe, X = Cl (**2.2**), X = I (**3.1**); M = Co, X = Cl (**2.3**), X = I (**2.4**); [PhBP$^{i\text{Pr}}_3$] = [PhB($CH_2P^iPr_2$)$_3$]$^-$).[9] The general routes for synthesizing N_2 complexes of Fe and Co are summarized in Scheme 5.3. Stirring a THF solution of an iodide complex [PhBP$^{i\text{Pr}}_3$]M—I in the presence of Mg turnings affords the zero-valent complex [(PhBP$^{i\text{Pr}}_3$)M(μ-N_2)]$_2$[Mg(THF)$_4$] (M = Fe (**3.3**), Co (**3.4**)) (Scheme 5.3). One electron reduction of a

divalent, chloride precursor [PhBP$^{i\mathrm{Pr}}_3$]M—Cl with Na/Hg amalgam yields the bridging N_2 complexes of the type ([PhBP$^{i\mathrm{Pr}}_3$]M)$_2$(μ-N_2) (M = Fe (**3.7**), Co (**3.8**)). The bridging N_2 complexes can be further reduced by one electron (Na/Hg) to afford formally mixed-valence species of the type [([PhBP$^{i\mathrm{Pr}}_3$]M)$_2$(μ-N_2)][Na(THF)$_6$] (M = Fe (**3.9**), Co (**3.10**)). Alternatively, the mixed valence complexes can be synthesized directly from the chloride precursor by reduction with excess Na/Hg amalgam (Scheme 5.3). The interconversion of these dinitrogen containing species is also possible as indicated in Scheme 5.1. Oxidation of the M^0 complexes [(PhBP$^{i\mathrm{Pr}}_3$)M(μ-N_2)]$_2$[Mg^{2+}] with two equivalents of ferrocenium generates the M^{I}—N_2—M^{I} complexes, while oxidation using one equivalent of ferrocenium generates the mixed-valent species M^{I}—N_2—M^0 (M = Fe or Co). Likewise, oxidation of the mixed-valent species M^{I}—N_2—M^0 with ferrocenium can generate the mixed valent species M^{I}—N_2—M^{I}, which can then itself be reduced to the mixed-valent species by reduction with Na/Hg amalgam.

5.2.2. Electrochemistry of ([PhBP$^{i\mathrm{Pr}}_3$]M)$_2$(μ-N_2) Complexes (M = Fe, Co). We have been able to chemically interconvert the N_2-bridged dimers between the neutral M^{I}—N_2—M^{I} and anionic, mixed valence [M^{I}—N_2—M^0]$^-$ states through one-electron reduction and one-electron oxidation reactions. The cyclic voltammetry of the N_2-dimer complexes was of obvious interest and has been studied in THF (Fc/Fc+, 0.4 M [^{n}Bu$_4$N][PF_6] or 0.4 M [^{n}Bu$_4$N][BPh_4], 75 mV/s). The data acquired are shown in Figure 5.1. Inspection of the electrochemical response of ([PhBP$^{i\mathrm{Pr}}_3$]Fe)$_2$(μ-N_2) (**3.7**) reveals a fully reversible redox process centered at -2.2 V and an irreversible oxidation at -0.9 V. We suggest that the reversible wave centered at -2.2 V of **3.7** corresponds to an $Fe^{I}Fe^{I}/Fe^0Fe^{I}$ redox process

and that the irreversible oxidation wave corresponds to an $Fe^{I}Fe^{II}/Fe^{I}Fe^{I}$ oxidation process. The dinitrogen ligand of the resulting $Fe^{I}Fe^{II}$ species should be prone to ligand substitution (chemical oxidation of **3.7** leads to a mixture of several metal-containing species). Repetitive scanning of **3.7** led to the growth of a new species detectable in the voltammogram. A fully reversible redox process grows in over several scans, centered at -2.0 V which is thought to be $[PhBP^{iPr}_3]FeF$ from activation of the PF_6^- electrolyte. However, this new species only arises after cycling past the oxidative wave at -0.9 V and does not appear with repetitive scanning about the reversible redox process centered at -2.2 V.

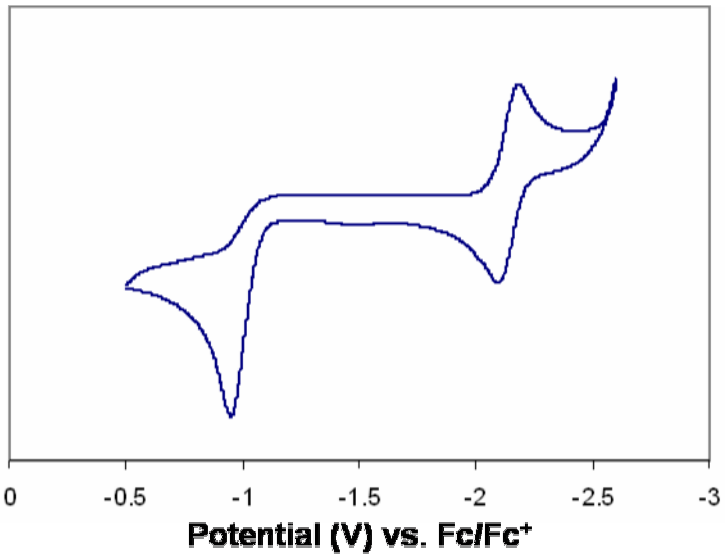

Figure 5.1. Cyclic voltammetry of $[PhBP^{iPr}_3]Fe)_2(\mu^2\text{-}N_2)$ (**3.7**) in 0.4 M $^{n}Bu_4NPF_6$/THF, scan rate 75 mV/s, V vs. Fc/Fc^+.

5.2.3. Structure. Theopold reported that for a series of coordinatively unsaturated tris(pyrazolyl)borate Co complexes ($[Tp^{Np}]Co—X$, where X = I, N_2, CO; $[Tp^{Np}]$ = hydrotris(2-neopentylpyrazolyl)borate), the capping ligand (X) may bend away from the

pseudo-threefold axis of the molecule, as defined by the vector from the boron atom to the metal center.[10] He rationalizes this tendency towards structural distortion to be a function of both the metal oxidation state and the nature of the capping ligand. For example, in the complex [Tp^{Np}]Co(CO), bending the carbonyl ligand away from the C_3 axis alleviates a σ* interaction between the Co d_z^2 orbital and the lone pair from the carbonyl ligand, while maximizing π-overlap between Co and the carbonyl π* orbitals by allowing the d_{xy} and $d_{x^2-y^2}$ orbital set to participate in bonding.

From our own laboratories, it has been observed within a family of [$PhBP^{Ph}_3$]Co—X complexes that the nature of the capping ligand will cause structural distortions from the expected tetrahedral geometries, and in some cases this distortion can even be accompanied by variations in the observed spin-states. Now we have isolated and structurally characterized [$PhBP^{iPr}_3$]M—X complexes with nitrogenous capping ligands in several oxidation states (M^0-M^{III}). We were thus interested in seeing what structural distortions these complexes may adopt as a function of their ground state electronic structure and the nature of the capping ligand. The molecular structures are shown for complexes **3.3**, **3.4**, **3.7**, **3.9**, and **3.10** in Figure 5.1 and their metric parameters are provided in Table 5.1.

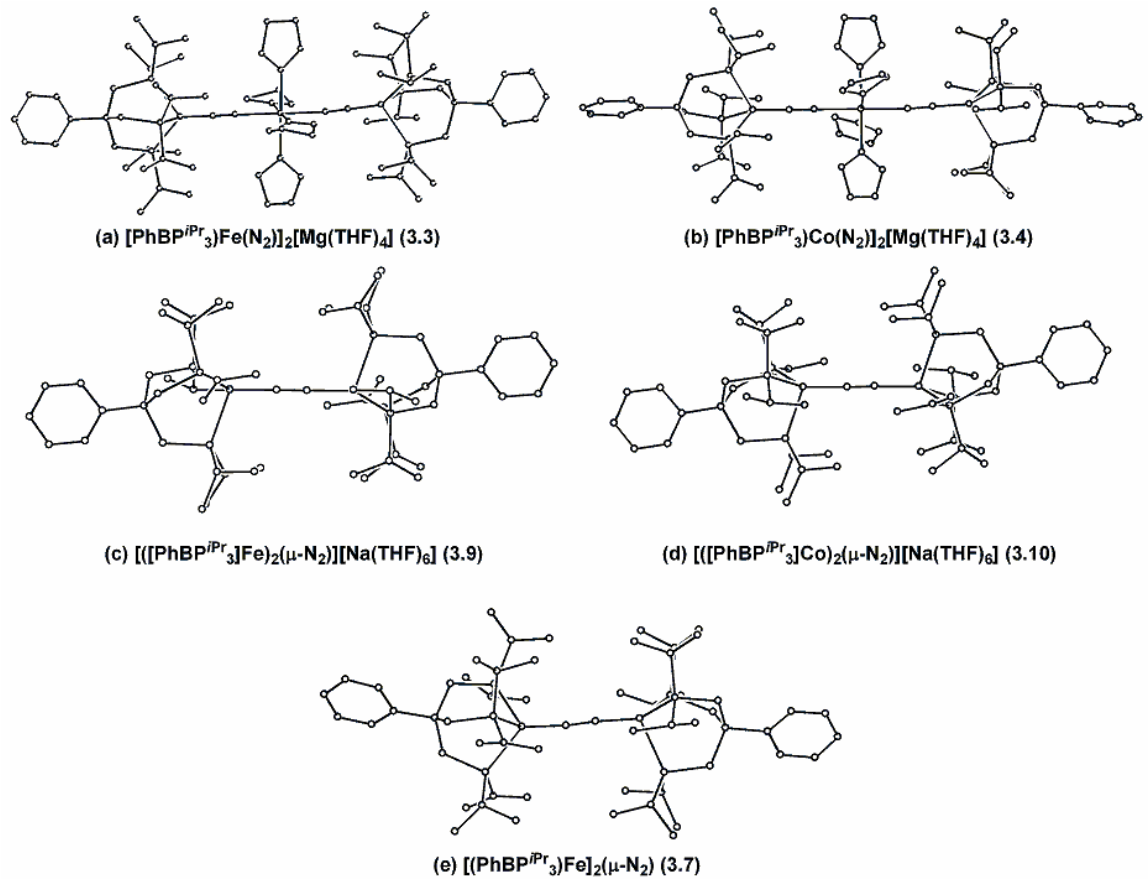

Figure 5.2. Molecular structures determined by X-ray diffraction studies of (a) [(PhBP$^{i\text{Pr}}_3$)Fe(N$_2$)]$_2$[Mg(THF)$_4$] (**3.3**), (b) [(PhBP$^{i\text{Pr}}_3$)Co(N$_2$)]$_2$[Mg(THF)$_4$] (**3.4**), (c) [([PhBP$^{i\text{Pr}}_3$]Fe)$_2$(μ-N$_2$)][Na(THF)$_6$] (**3.9**), (d) [([PhBP$^{i\text{Pr}}_3$]Co)$_2$(μ-N$_2$)][Na(THF)$_6$] (**3.10**), and (e) ([PhBP$^{i\text{Pr}}_3$]Fe)$_2$(μ-N$_2$) (**3.7**). Cations (for anionic structures), solvent molecules, and hydrogen atoms have been omitted for clarity.

Table 5.1. Relevant bond distances and angles for specified complexes.

#	Distances (Å)				Angles(°)				
	X-M	M-P		N_α-N_β	α^1	X-M-P		P-M-P	
3.3	N_α, 1.686	P1	2.293	1.158	16	P1	114	P1, P2	96.7
		P2	2.311			P2	137	P1, P3	94.0
		P3	2.286			P3	111	P2, P3	95.5
3.4	N_α, 1.687	P1	2.274	1.155	10	P1	117	P1, P2	93.2
		P2	2.211			P2	117	P1, P3	95.8
		P3	2.259			P3	132	P2, P3	93.4
3.7	N_α, 1.815	P1	2.350	1.138	12	P1	113	P1, P2	96.9
		P2	2.394			P2	113	P1, P3	97.0
		P3	2.340			P3	136	P2, P3	93.8
3.9	N_α, 1.813	P1	2.292	1.171	12	P1	119	P1, P2	96.9
		P2	2.278			P2	110	P1, P3	98.0
		P3	2.290			P3	130	P2, P3	97.2
3.10	N_α, 1.805	P1	2.232	1.147	15	P1	133	P1, P2	95.1
		P2	2.230			P2	123	P1, P3	93.6
		P3	2.249			P3	108	P2, P3	93.5
4.3	N, 1.953	P1	2.462	--	6	P1	128	P1, P2	92.8
		P2	2.467			P2	125	P1, P3	91.7
		P3	2.443			P3	117	P2, P3	93.7
3.11	N, 1.638	P1	2.260	--	6	P1	122	P1, P2	91.1
		P2	2.297			P2	130	P1, P3	91.6
		P3	2.263			P3	120	P2, P3	92.4

[1] α defined as angle B-M-X, or deviation of M—X from the B—M vector.

Figure 5.3 displays the ligand distortions observed for four-coordinate complexes featuring the [$PhBP^{iPr}_3$] ligand. Structure type (a) represents a C_3 symmetric structure type where the M—X bond axis lies along the B—M axis. Structure type (b) shows the deviation of the M—X bond by some angle α from the B—M vector. This structure type can be generally considered trigonal-monopyramidal, where the two eclipsed PR_2 groups and the X ligand make the base of the pyramid. Structure type (c) occurs when α = 54.7 °, ligand X is effectively *trans* to one of the phosphine donors and the geometry is best described as a *cis*-divacant octahedron.

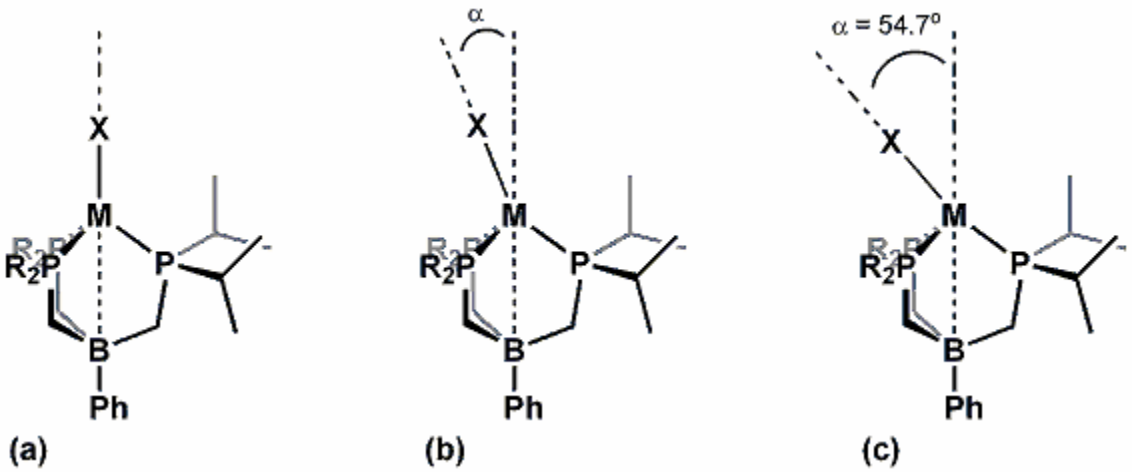

Figure 5.3 Limiting structure types for four-coordinate "[PhBP$^{i\text{Pr}}_3$]M" species: (a) tetrahedral (α = 0º), (b) trigonal-monopyramidal, (c) *cis*-divacant octahedral (α = 54.7º).

The bond distances, angles, and deviation parameter α are provided for the complexes in Figure 5.3. The analogous Fe and Co complexes (e.g., M^0 complexes **3.3** and **3.4**) exhibit very similar metric parameters (see Table 5.1). Thus, we will limit our discussion to the Fe subset and examine the structure types as a function of oxidation state and capping ligand. The Fe complexes [PhBP$^{i\text{Pr}}_3$]FeNPh$_2$ (**4.3**) and [PhBP$^{i\text{Pr}}_3$]FeNAd (**3.11**) have been included in this comparison as representative Fe^{II} and Fe^{III} species where the capping ligand is a nitrogenous functionality.

Figure 5.4 shows the immediate coordination environment for compounds [(PhBP$^{i\text{Pr}}_3$)Fe(μ-N$_2$)]$_2$[Mg(THF)$_4$] (**3.3**), ([PhBP$^{i\text{Pr}}_3$]Fe)$_2$(μ-N$_2$) (**3.7**), [PhBP$^{i\text{Pr}}_3$]FeNPh$_2$ (**4.3**), and [PhBP$^{i\text{Pr}}_3$]FeNAd (**3.11**). The threefold axis, defined by the B—M vector, is indicated by a dashed line in the figures. There is very little observable bending (α = 6º) in the Fe—N bond in the high-spin, (*S* = 2) [PhBP$^{i\text{Pr}}_3$]FeNPh$_2$ structure (Figure 5.4 c). This is not surprising, given that no significant π-bonding occurs between the metal and the NPh$_2$ group. The Fe^{III} imide **3.11**, which has two strong Fe—N π-bonds, also shows

little evidence of bending (α = 6º) of the imide fragment from the B—Fe vector. The Fe—X bond is noticeably bent, however, in the Fe^0 (S = 1, α = 16º) and Fe^I (S = 3/2, α = 12º) structures (Figure 5.4 a,b). In the following discussion, these observations will be rationalized based upon the nature of the bonding in the M—N linkage.

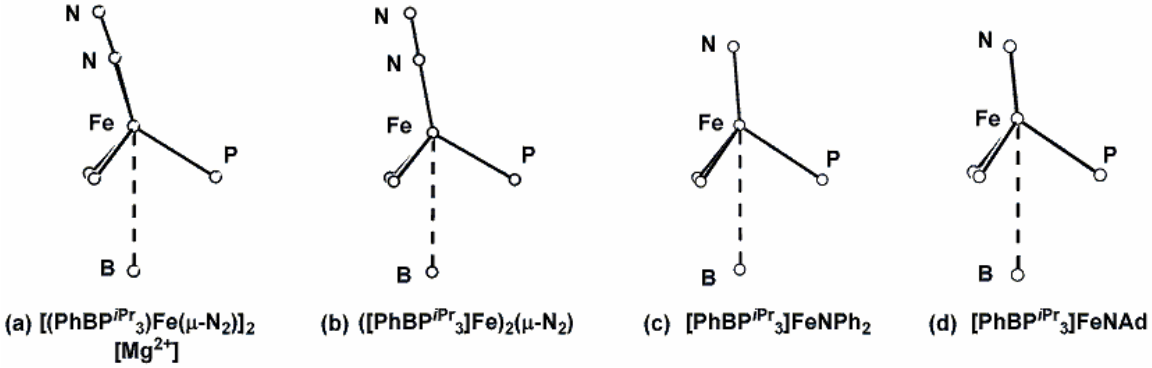

Figure 5.4. The core structure representations for (a) Fe^0 (S = 1) in **3.3**, (b) Fe^I (S = 3/2) in **3.7**, (c) Fe^{II} (S = 2) in **4.3**, and (d) Fe^{III} (S = 1/2) in **3.11**.

5.2.4. Bonding Geometries and Molecular Orbital Considerations. We observed in the previous section that a geometry distortion occurs in the N_2-containing complexes. The distortion involves the M—N_2 bond vector bending away from the molecule's threefold axis, defined by the B—M vector. The bending distortion reduces the symmetry of the molecule from C_3 to C_s symmetry and causes two significant changes in the nature of the M—N_2 bonding interaction (Figure 5.5). (1) Bending the M—N_2 linkage from the threefold axis reduces the σ* interaction between the nitrogen lone pair and the d_z^2 on the metal, which are both filled for Fe^0 (d^8) in **3.3** and Co^0 (d^9) in **3.4**. (2) In C_s symmetry, the two degenerate e sets in C_3 symmetry split to permit mixing of the lower e-set orbital components (i.e., $d_{x^2-y^2}$ and d_{xy}). While bending the dinitrogen ligand away from the

threefold axis reduces the metal-N_2 π-overlap in 2a", π-bonding character develops between the N_2 π* orbital and the metal 1a" orbital. As mentioned in Section 5.2, the Fe^{III} imide **3.11** does not exhibit any bending of the Fe—N linkage. Significant contribution from the overlying Fe p orbital hybridizes the d_z^2 orbital to alleviate the Fe—N σ* interaction.[11]

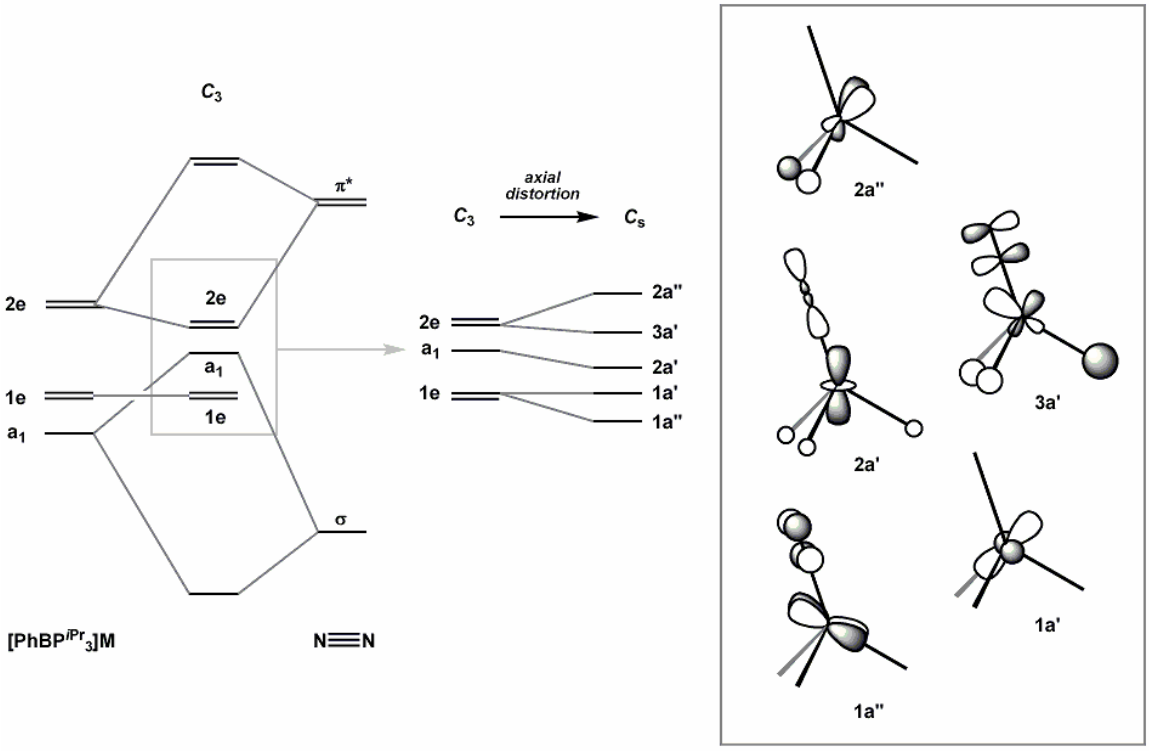

Figure 5.5. Molecular orbital bonding diagram for species of the type $[PhBP^{iPr}_3]M—N_2$ (M = Fe, Co).

A similar treatment of the dinitrogen bridged complexes of the type $([PhBP^{iPr}_3]M)_2(\mu\text{-}N_2)$ produces the molecular orbital diagram presented in Figure 5.6. The bending distortion is lessened in these bimetallic systems (Table 5.1 and Figure 5.2), though it is still observed. As an approximation, the bimetallic core can be transformed with S_6 symmetry.[4b] The orbital interactions representing M—N_2—M bonding

interactions ($2a_g$ and $2e_g$) are illustrated in the inset of Figure 5.6. Bending the M—N_2 off the threefold axis decreases the σ* interaction depicted in $2a_g$. However, the bending distortion observed is not large enough to suggest that significant mixing of the lower e-set ($1e_g$, $1e_u$) is mixing into the bonding interactions.

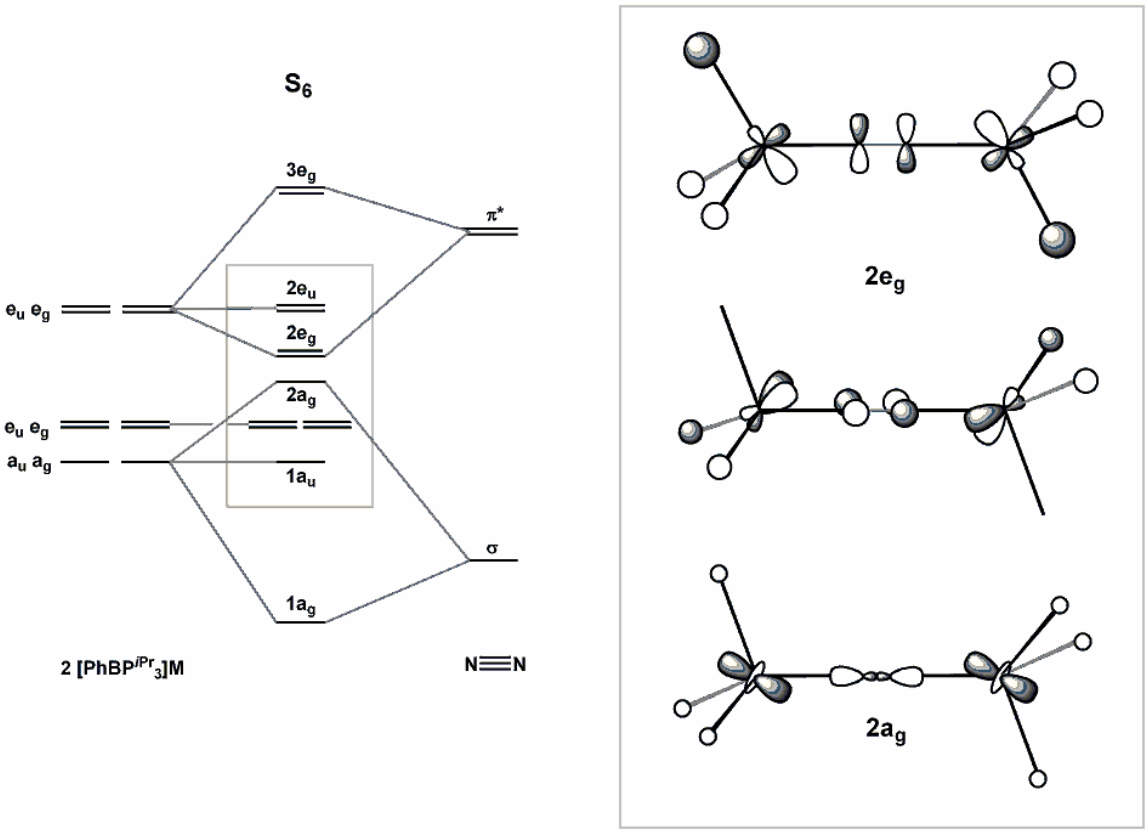

Figure 5.6. Molecular orbital bonding diagram for species of the type $([PhBP^{iPr}_3]M)_2(\mu\text{-}N_2)$ (M = Fe, Co).

5.2.5. Magnetic Characterization of $[PhBP^{iPr}_3]M(\mu\text{-}N_2)M'$ Complexes (M = Fe, Co, M' = Fe, Co, Mg). Solid-state magnetic susceptibility data for the zero-valent complexes (i.e., $[(PhBP^{iPr}_3)M(\mu\text{-}N_2)]_2[Mg^{2+}]$) **3.3** and **3.4** were obtained from 4 to 300 K by SQUID magnetometry and are plotted, per dimeric unit, in Figures 5.7 a-d. The average μ_{eff}

observed for **3.3** over the temperature range of 60-300 K is 5.63 BM, higher than the spin-only value for four unpaired electrons (4.90 BM). As can be seen from the plot of χ_m^{-1} vs T (Figure 5.7 b), the Curie Law is observed, indicating each Fe in **3.3** maintains its triplet ground state (S = 1) throughout the entire temperature range of 4-300 K investigated. The same qualitative observations can be made for its Co congener **3.4**. As shown in Figure 5.7 c, **3.4** exhibits an average μ_{eff} of 4.16 B.M. (60-300 K). Complex **3.4** also maintains its triplet ground state throughout the entire temperature range of 4-300 K investigated as evidenced by the plot of χ_m^{-1} vs. T (Figure 5.7 d). That both dimers **3.3** and **3.4** have average moments higher than the corresponding spin-only values for four and two unpaired electrons suggests significant spin-orbit coupling is occurring.

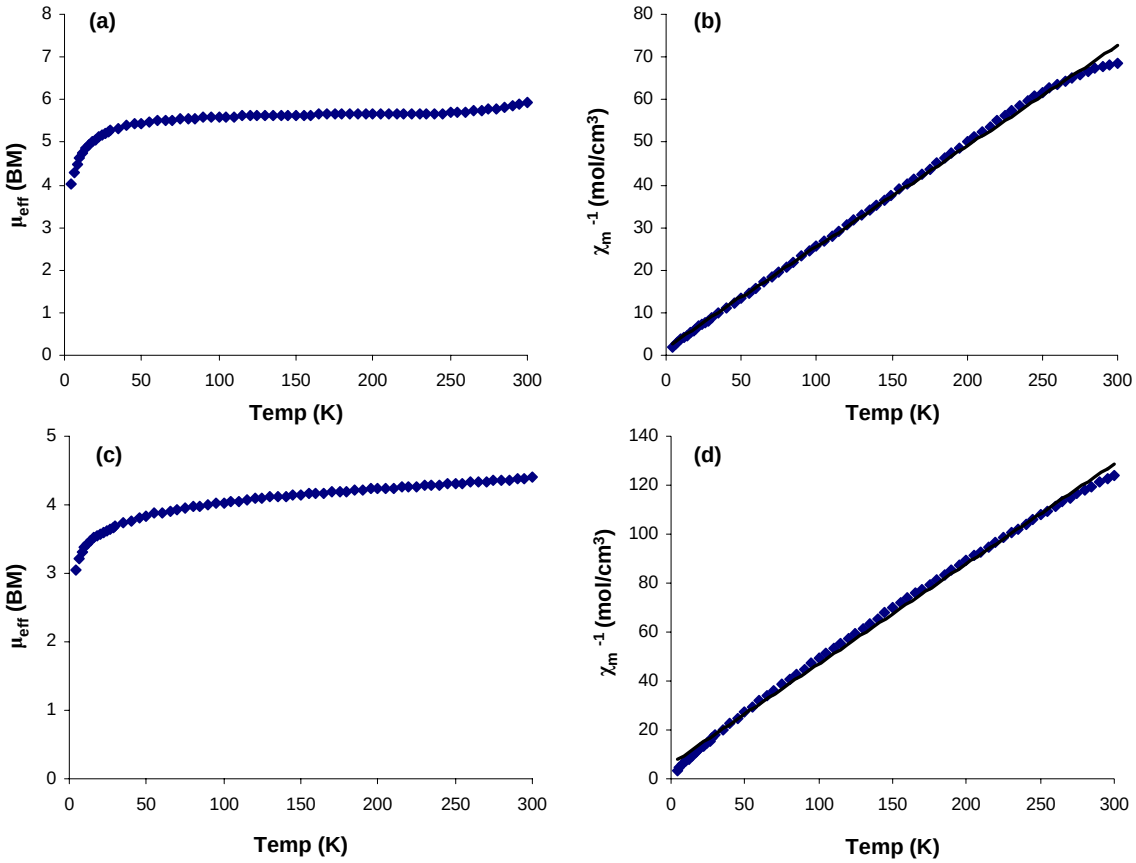

Figure 5.7. (a) SQUID magnetization data shown as a plot of μ_{eff} versus T, and (b) as a plot of χ_m^{-1} versus T, for $[(PhBP^{iPr}_3)Fe(\mu\text{-}N_2)]_2[Mg(THF)_4]$ (**3.3**); (c) μ_{eff} versus T, and (d) as a plot of χ_m^{-1} versus T, for $[(PhBP^{iPr}_3)Co(\mu\text{-}N_2)]_2[Mg(THF)_4]$ (**3.4**).

The recently characterized bridging nitride complex $[([PhBP^{Ph}_3]Fe)_2(\mu\text{-}N)][Na(THF)_5]$ is comprised of two high-spin Fe^{II} nuclei that are antiferromagnetically coupled to yield a ground state $S = 0$, diamagnetic species.[11] Thus, we were interested if any of the dinitrogen-bridged species would exhibit similar antiferromagnetic coupling across the N_2-bridge. Solid-state magnetic susceptibility data for $([PhBP^{iPr}_3]Fe)_2(\mu\text{-}N_2)$ (**3.7**), $[([PhBP^{iPr}_3]Fe)_2(\mu\text{-}N_2)][Na(THF)_6]$ (**3.9**), and $[([PhBP^{iPr}_3]Co)_2(\mu\text{-}N_2)][Na(THF)_6]$ (**3.10**) were obtained from 4 to 300 K by SQUID magnetometry and are plotted, per dimeric unit, in Figures 5.8 a-f.[12]

Unlike the bridging nitride complex,[11] all of the cases examined here remain rigorously ferromagnetically coupled. The Curie Law is obeyed for each complex (Figure 5.8 b,d,f), indicating that a single spin-state (per complex) is maintained over the range of temperatures examined. For the Fe mixed valence complex **3.9**, an average μ_{eff} of 7.40 B.M. is observed for the $S = 5/2$ system. For the Co congener **3.10**, an average μ_{eff} of 4.37 B.M. is observed for the $S = 3/2$ system. Like the zero-valent species **3.3** and **3.4**, both **3.9** and **3.10** show evidence that spin-orbit coupling is occurring, for both their average μ_{eff} values exceed the spin-only values for five (5.92 B.M.) and three (3.87 B.M.) unpaired electrons, respectively. Curiously, however, the neutral, $S = 3$ Fe^{I} dimer **3.7** exhibits a lower average μ_{eff} value (7.02 B.M.) than the $S = 5/2$ complex **3.9**. This difference may be attributable to the degree of spin-orbit coupling on going from an integer spin-system (**3.7**) to a 5/2 spin-system (**3.9**), or that the odd spin in the latter complex could potentially be localized on the dinitrogen ligand to create a three-spin problem (i.e., Fe^{I}—(N_2^{-})—Fe^{I}).

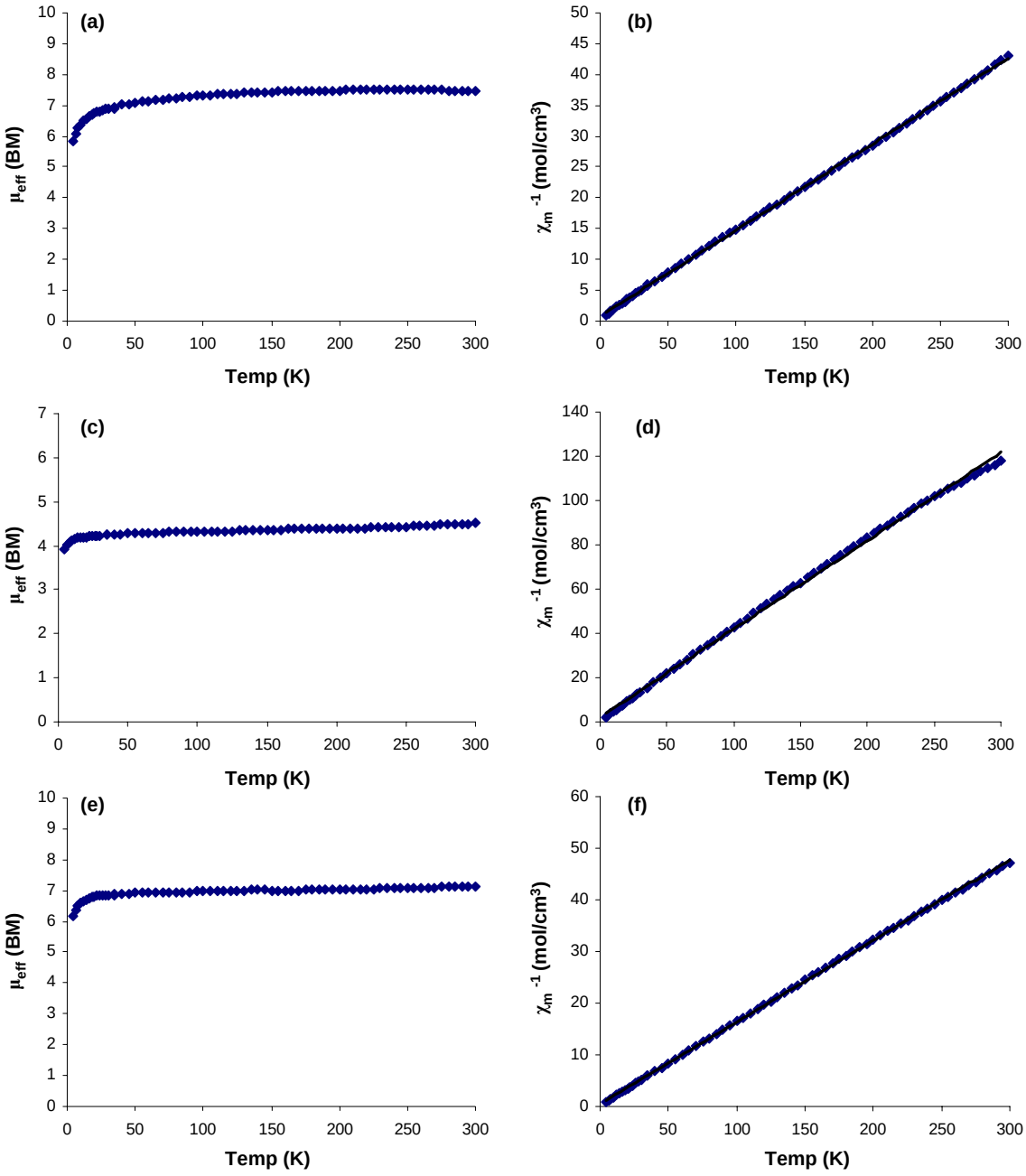

Figure 5.8. (a) SQUID magnetization data shown as a plot of μ_{eff} versus T, and (b) as a plot of χ_m^{-1} versus T, for [([PhBP$^{i\text{Pr}}_3$]Fe)$_2$(μ-N$_2$)][Na(THF)$_6$] (**3.9**); (c) μ_{eff} versus T, and (d) as a plot of χ_m^{-1} versus T, for [([PhBP$^{i\text{Pr}}_3$]Co)$_2$(μ-N$_2$)][Na(THF)$_6$] (**3.10**); (e) μ_{eff} versus T, and (f) as a plot of χ_m^{-1} versus T, for [PhBP$^{i\text{Pr}}_3$]Fe(μ-N$_2$) (**3.7**).

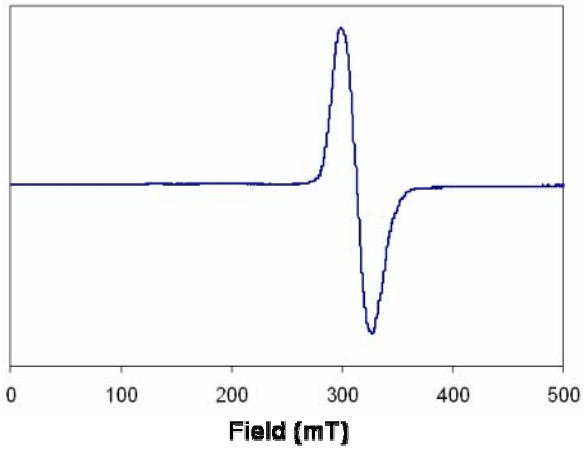

Figure 5.9. EPR spectrum of $[(PhBP^{iPr}_3)Co(\mu\text{-}N_2)]_2[Mg(THF)_4]$ (**3.4**) in glassy THF (4 K, X-band, 9.62 GHz).

The EPR spectra for the zero-valent complex $[(PhBP^{iPr}_3)Co(\mu\text{-}N_2)]_2[Mg(THF)_4]$ (**3.4**) in a THF glass at 4 K is shown in Figure 5.9. The S = ½ Co^0 complex, (**3.4**), displays an isotropic signal centered at g = 2.2 (h = 313 mT). The isotropic signal persists for temperatures up to 60 K but then disappears at temperatures exceeding 60 K.

The mixed-valence Co dimer $[([PhBP^{iPr}_3]Co)_2(\mu\text{-}N_2)][Na(THF)_6]$ (**3.10**) exhibits a temperature dependent EPR signal, as shown in Figure 5.10 a,b. The three g tensors (5.16, 3.26, and 2.04) are resolvable for the $S = {}^3/_2$ Co dimer **3.10** at 20 K (Figure 5.10 a)**.** The g tensors remain resolvable up to 60 K, but as in the case of **3.4**, the signal fades at temperatures exceeding 60 K. Although the spin-state does not appear to be changing as a function of temperature (i.e., there does not appear to be a signal for an S = ½ state), the intensities of the spectral features do change with temperature.

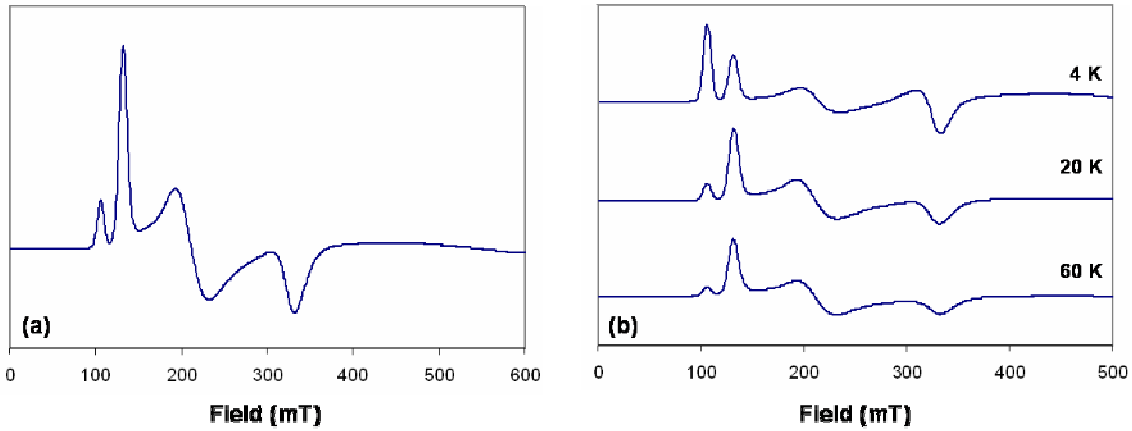

Figure 5.10. (a) EPR spectrum of [([PhBP$^{i\text{Pr}}_3$]Co)$_2$(μ-N$_2$)][Na(THF)$_6$] (**3.10**) in glassy THF (20 K, X-band, 9.62 GHz), and (b) EPR spectra of **3.10** taken at (top) 4 K, (middle) 20 K, and (bottom) 60 K.

The mixed-valence Fe dimer [([PhBP$^{i\text{Pr}}_3$]Fe)$_2$(μ-N$_2$)][Na(THF)$_6$] (**3.9**) also exhibits a temperature dependent EPR signal, as shown in Figure 5.11 a,b. The three g tensors (6.01, 3.17, and 2.01) are resolvable for the $S = {}^5/_2$ Fe dimer **3.9** at 20 K (Figure 5.11 a)**.** While the gross spectral features for **3.9** are maintained in the spectra taken at 4, 20, and 60 K, the features change more considerably as a function of temperature than in the Co example. A possible reason for this observation is that the features of the $S = {}^5/_2$ state shift with temperature; or alternatively, it is possible that multiple electronic states (e.g., $S = {}^3/_2$, $S = {}^5/_2$) are being populated at the lower temperature studied.

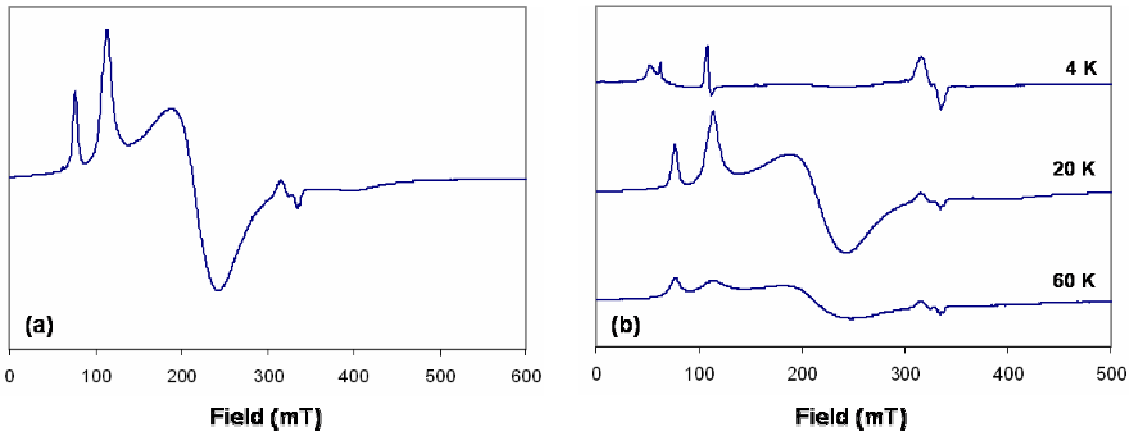

Figure 5.11. (a) EPR spectrum of [([PhBP$^{iPr}_3$]Fe)$_2$(μ-N$_2$)][Na(THF)$_6$] (**3.9**) in glassy THF (20 K, X-band, 9.62 GHz), and (b) EPR spectra of **3.9** taken at (top) 4 K, (middle) 20 K, and (bottom) 60 K.

5.2.6. Electronic Structure for Monomer and Dimer Complexes. The SQUID data acquired for the all the complexes in this study indicate that each complex maintains its spin state at all temperatures examined. For the dimeric cases (**3.7**-**3.10**), this means the complexes remain ferromagnetically coupled at all temperatures observed.[12] The EPR for the Fe mixed-valence complex **3.9** may indicate some spin-state mixing as a function of temperature, but the SQUID data does not suggest that the complex is antiferromagnetically coupled at any temperature.

The complexes presented in this chapter, as well as those in the accompanying chapters, can fall into two general structure types: monomeric and dimeric species. For the monomer subclass, we have now isolated "[PhBP$^{iPr}_3$]M" species in 5 spin states (S = 0-2), spanning five oxidation states for Fe and four oxidation states for Co. Examples of these complexes are presented in Figure 5.12. The generalized complexes in Figure 5.12 are featured in C_3 symmetric ligand fields. Worth noting is that for the M^{III} imide structures, the d_z^2 orbital decreases in energy to aid in stabilizing the metal-imide

frameworks. However, upon going to a terminal nitride ligand, the d_z^2 orbital raises significantly enough in energy to force a singlet ground state.

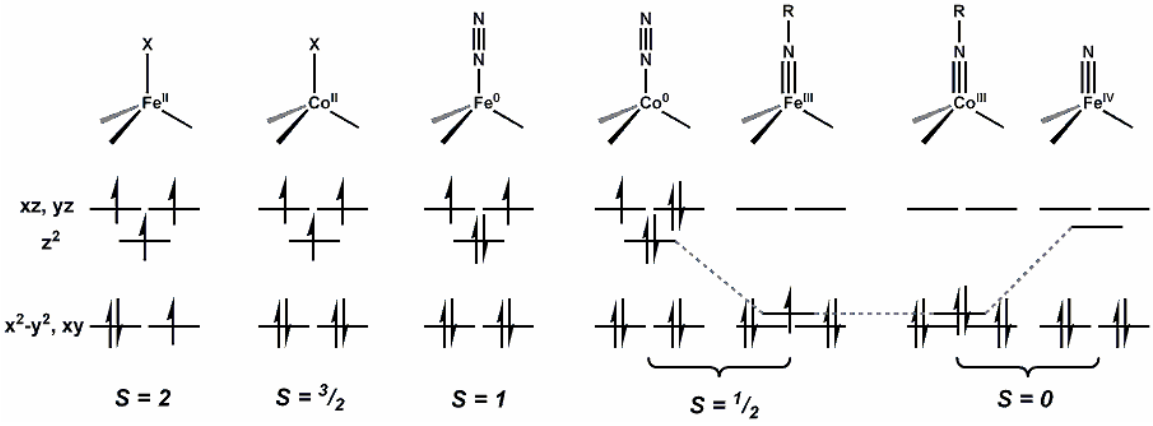

Figure 5.12. The ground state electronic structures observed for mononuclear Fe and Co complexes at various oxidation states. In general, the complexes are simplified to C_3 symmetry to provide a general ordering of the bonding orbital interactions.

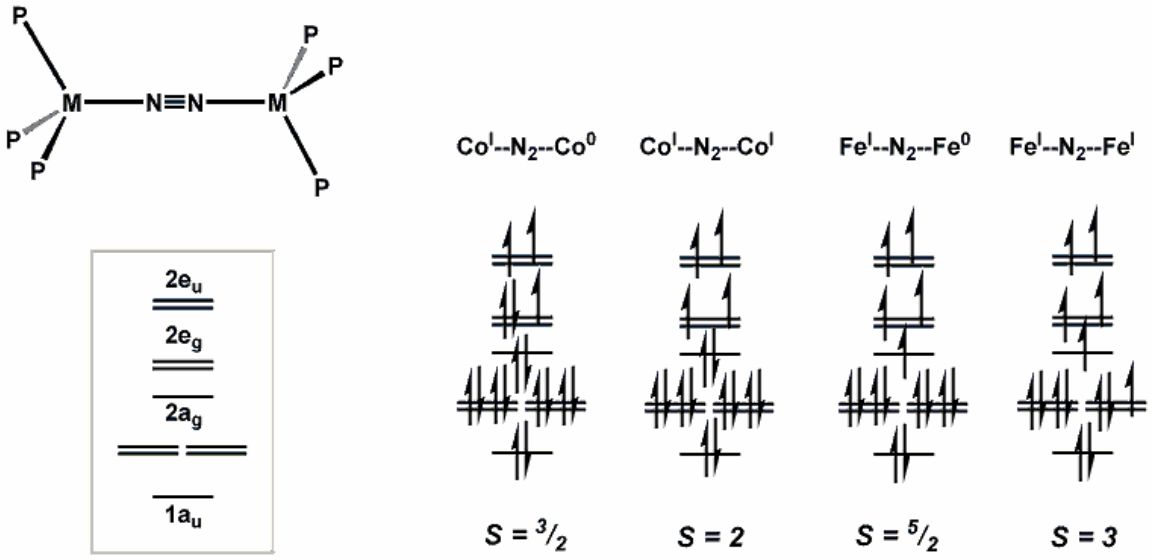

Figure 5.13. The ground state electronic structures observed for dinitrogen-bridged, dinuclear species. In general, the complexes are simplified to S_6 symmetry to provide a general ordering of the bonding orbital interactions.

Figure 5.12 summarizes how using the [PhBP$^{i\text{Pr}}_3$] ligand framework has allowed us to traverse spin-states from S = 0 to S = 2 while spanning a wide range of metal oxidation states. In much the same fashion, we have demonstrated that the [PhBP$^{i\text{Pr}}_3$]M—N_2—M[PhBP$^{i\text{Pr}}_3$] framework also can stabilize a wide range of spin-states. As summarized in Figure 5.13, the four spin states (S = $^3/_2$ to S = 3) are depicted for the ferromanetically-coupled complexes **3.7**-**3.10**.

5.3. Conclusions.

These data allow us to summarize several salient features of the chemistry described herein. The [PhBP$^{i\text{Pr}}_3$] ligand can support a single iron or cobalt center in a pseudo-tetrahedral environment in which dinitrogen is bound in the fourth coordination site. While the zero-valent metal-dinitrogen complexes have the general formula [([PhBP$^{i\text{Pr}}_3$]M(μ-N_2)]$_2$[Mg^{2+}] (M = Fe, Co), bridging structures can also be obtained as neutral [M^{I}]—N_2—[M^{I}] complexes, or as their reduced anions [M^{I}]—N_2—[M^{0}] ([M] = [PhBP$^{i\text{Pr}}_3$]Fe, [PhBP$^{i\text{Pr}}_3$]Co). The latter mixed-valence compounds exhibit delocalization of the anionic charge, as evidenced by their crystallographic behavior and lack of υ_{NN} in the IR spectra. The structural distortions exhibited by both [([PhBP$^{i\text{Pr}}_3$]M(μ-N_2)]$_2$[Mg^{2+}] and [M^{n}]—N_2—[M^{n}] complexes minimize σ* interactions between the M d_z^2 and nitrogen lone pair, while lowering the overall molecular symmetry and allowing admixing of the metal d orbitals to maximize π-overlap with the π* dinitrogen orbitals. Magnetic characterization of the neutral and mixed-valence dimeric complexes reveal the complexes remain ferromagnetically coupled over all temperatures investigated.

5.4. Experimental Section

5.4.1 General Considerations. All manipulations were carried out using standard Schlenk or glove-box techniques under a dinitrogen atmosphere. Unless otherwise noted, solvents were deoxygenated and dried by thorough sparging with N_2 gas followed by passage through an activated alumina column. Non-halogenated solvents were typically tested with a standard purple solution of sodium benzophenone ketyl in tetrahydrofuran in order to confirm effective oxygen and moisture removal. Deuterated solvents were degassed and stored over activated 3-Å molecular sieves prior to use. THF-d_8 was dried by passage over activated alumina and stored over activated sieves prior to use. [PhBP$^{i\text{Pr}}_3$][Tl] (**2.1**), [PhBP$^{i\text{Pr}}_3$]FeCl (**2.2**), [PhBP$^{i\text{Pr}}_3$]CoCl (**2.3**), [PhBP$^{i\text{Pr}}_3$]FeI (**3.1**), [PhBP$^{i\text{Pr}}_3$]CoI (**2.4**), [(PhBP$^{i\text{Pr}}_3$)Fe(N_2)]$_2$[Mg(THF)$_4$] (**3.3**), [(PhBP$^{i\text{Pr}}_3$)Co(N_2)]$_2$[Mg(THF)$_4$] (**3.4**), ([PhBP$^{i\text{Pr}}_3$]Fe)$_2$(μ-N_2) (**3.7**), ([PhBP$^{i\text{Pr}}_3$]Co)$_2$(μ-N_2) (**3.8**), [([PhBP$^{i\text{Pr}}_3$]Fe)$_2$(μ-N_2)][Na(THF)$_6$] (**3.9**), [([PhBP$^{i\text{Pr}}_3$]Co)$_2$(μ-N_2)][Na(THF)$_6$] (**3.10**), [PhBP$^{i\text{Pr}}_3$]FeNPh$_2$ (**4.3**), and [PhBP$^{i\text{Pr}}_3$]FeNAd (**3.11**) were prepared as previously reported in the previous chapters. All reagents were purchased from commercial vendors and used without further purification unless explicitly stated. Elemental analyses were carried out at Desert Analytics, Tucson, Arizona. NMR spectra were recorded at ambient temperature on Varian Mercury 300 MHz, Joel 400 MHz, and Inova 500 MHz spectrometers, unless otherwise noted. ^{1}H NMR chemical shifts were referenced to residual solvent. ^{31}P NMR chemical shifts are reported relative to an external standard of 85% H_3PO_4. IR spectra were recorded on a Bio-Rad Excalibur FTS 3000 spectrometer controlled by Win-IR Pro software. UV-vis measurements were taken on a Hewlett Packard 8452A diode array spectrometer using a quartz crystal cell with a Teflon cap. X-

ray diffraction studies were carried out in the Beckman Institute Crystallographic Facility on a Bruker Smart 1000 CCD diffractometer.

5.4.2 X-ray Crystallography Procedures. X-ray quality crystals were grown as indicated in the experimental procedures for each complex. The crystals were mounted on a glass fiber with Paratone-N oil. Structures were determined using direct methods with standard Fourier techniques using the Bruker AXS software package. In some cases, Patterson maps were used in place of the direct methods procedure.

5.4.3. Magnetic Measurements. Measurements were recorded using a Quantum Designs SQUID magnetometer running MPMSR2 software (Magnetic Property Measurement System Revision 2). Data were recorded at 5000 G. Samples were suspended in the magnetometer in plastic straws sealed under nitrogen with Lilly No. 4 gel caps. Loaded samples were centered within the magnetometer using the DC centering scan at 35 K and 5000 gauss. Data were acquired at 2-10 K (one data point/2 K), 10-60 K (one data point/5 K), and 60-310 K (one data point/10 K).

$$\chi_m = (\chi M)/(mG) \qquad (\mathbf{5.1})$$

$$\mu_{eff} = \mathrm{SQRT}(7.997\chi_m T) \qquad (\mathbf{5.2})$$

The magnetic susceptibility was adjusted for diamagnetic contributions using the constitutive corrections of Pascal's constants and a fixed temperature independent paramagnetism (TIP) crudely set to 2×10^{-4} cm^3 mol^{-1}.[13] The molar magnetic susceptibility (χ_m) was calculated by converting the calculated magnetic susceptibility (χ) (or magnetization) obtained from the magnetometer to a molar susceptibility using the multiplication factor [molecular weight (M)]/[sample weight (m) × field strength (G)]). Curie-Weiss behavior was verified by a plot of χ_m^{-1} versus T. Data were analyzed using

equations 5.1 and 5.2. Average magnetic moments were taken from the average of magnetic moments from the ranges indicated in the Experimental Section for each complex. The Weiss constant (χ) was taken as the *x*-intercept of the plot of χ_m^{-1} versus *T*. Error bars were established at 95% confidence using regression analysis or taking two standard deviations from the mean. Solution magnetic moments were measured by the Evans method and were adjusted for diamagnetic contributions using the constitutive corrections of Pascal's constants. Averaged *g*-factors can be extracted from the susceptibility data, assuming zero orbital contributions, using the following equation 5.3.

$$\chi_m = (Ng^2\beta^2)/(3\,kT)\,(S(S+1)) \qquad \textbf{(5.3)}$$

5.4.4. EPR Measurements. X-band EPR spectra were obtained on a Bruker EMX spectrometer equipped with a rectangular cavity working in the TE_{102} mode. Variable temperature measurements were conducted with an Oxford continuous-flow helium cryostat (temperature range 3.6-300 K). Accurate frequency values were provided by a frequency counter built in the microwave bridge. Solution spectra were acquired in toluene for all of the complexes. Sample preparation was performed under a nitrogen atmosphere.

References Cited

1. MacKay, B. A.; Fryzuk, M. D. *Chem Rev*. **2004**, *104*, 385.

2. (a) Schrock, R. R. *Acc. Chem. Res.* **1997**, *30*, 9. (b) Peters, J. C.; Cherry, J.-P. F.; Thomas, J. C.; Baraldo, L.; Mindiola, D. J.; Davis, W. M.; Cummins, C. C. *J. Am. Chem. Soc.* **1999**, *121*, 10053. (c) Yandulov, D. V.; Schrock. R. R. *Science* **2003**, *301*, 76.

3. (a) Dititanium μ-dinitrogen complexes: (a) Berry, D. H.; Procopio, L. J.; Carroll, P. J. *Organometallics* **1988**, *7*, 570. (b) Duchateau, R.; Gambarotta, S.; Beydoun, N.; Bensimon, C. *J. Am. Chem. Soc.* **1991**, *113*, 8986. (c) Beydoun, N.; Duchateau, R.; Gambarotta, S. *J. Chem. Soc., Chem.Commun.* **1992**, 244. (d) Sanner, R. D.; Duggan, D. M.; McKenzie, T. C.; Marsh, R. E.; Bercaw, J. E. *J. Am. Chem. Soc.* **1976**, *98*, 8358. (e) Zeinstra, J. D.; Teuben, J. H.; Jellinek, F. *J. Organomet. Chem.* **1979**, *170*, 39. Dizirconium *í*-dinitrogen complexes: (f) Sanner, R. D.; Manriquez, J. M.; Marsh, R. E.; Bercaw, J. E. *J. Am. Chem. Soc.* **1976**, *98*, 8351. (g) Fryzuk, M. D.; Haddad, T. S.; Mylvaganam, M.; McConville, D. H.; Rettig, S. J. *J. Am. Chem. Soc.* **1993**, *115*, 2782. (h) Cohen, J. D.; Mylvaganam, M.; Fryzuk, M. D.; Loehr, T. M. *J. Am. Chem. Soc.* **1994**, *116*, 9529. Divanadium μ-dinitrogen complexes: (i) Edema, J. J. H.; Meetsma, A.; Gambarotta, S. *J. Am. Chem. Soc.* **1989**, *111*, 6878. (j) Song, J.-I.; Berno, P.; Gambarotta, S. *J. Am. Chem. Soc.* **1994**, *116*, 6927. (k) Berno, P.; Hao, S.; Minhas, R.; Gambarotta, S. *J. Am. Chem. Soc.* **1994**, *116*, 7417. (l) Buijink, J.-K. F.; Meetsma, A.; Teuben, J. H. *Organometallics* **1993**, *12*, 2004. (m) Ferguson, R.; Solari, E.; Floriani, C.; Chiesi-Villa, A.; Rizzoli, C. *Angew. Chem., Int. Ed. Engl.* **1993**, *32*, 396. Diniobium μ-dinitrogen complexes: (n) Dilworth, J. R.; Henderson, R. A.; Hills, A.; Hughes, D. L.; Macdonald, C.; Stephens, A. N.; Walton, D. R. M. *J. Chem. Soc., Dalton Trans.* **1990**, 1077. (o)

Berno, P.; Gambarotta, S. *Organometallics* **1995**, *14*, 2159. Ditantalum μ-dinitrogen complexes: (p) Turner, H. W.; Fellmann, J. D.; Rocklage, S. M.; Schrock, R. R.; Churchill, M. R.; Wasserman, H. J. *J. Am. Chem. Soc.* **1980**, *102*, 7809. (q) Rocklage, S. M.; Turner, H. W.; Fellmann, J. D.; Schrock, R. R. *Organometallics* **1982**, *1*, 703. (r) Rocklage, S. M.; Schrock, R. R. *J. Am. Chem. Soc.* **1982**, *104*, 3077. (s) Churchill, M. R.; Wasserman, H. J. *Inorg. Chem.* **1981**, *20*, 2899. (t) Churchill, M. R.; Wasserman, H. J. *Inorg. Chem.* **1982**, *21*, 218. (u) Schrock, R. R.; Wesolek, M.; Liu, A. H.; Wallace, K. C.; Dewan, J. C. *Inorg. Chem.* **1988**, *27*, 2050. Dichromium *í*-dinitrogen complexes: (v) Denholm, S.; Hunter, G.; Weakley, T. J. R. *J. Chem. Soc., Dalton Trans.* **1987**, 2789. Dimolybdenum μ-dinitrogen complexes: (w) Forder, R. A.; Prout, K. *Acta Crystallogr.* **1974**, *B30*, 2778. (x) Schrock, R. R.; Kolodziej, R. M.; Liu, A. H.; Davis, W. M.; Vale, M. G. *J. Am. Chem. Soc.* **1990**, *112*, 4338. (y) Kol, M.; Schrock, R. R.; Kempe, R.; Davis, W. M. *J. Am. Chem. Soc.* **1994**, *116*, 4382. (z) Shih, K.-Y.; Schrock, R. R.; Kempe, R. *J. Am. Chem.Soc.* **1994**, *116*, 8804. (aa) Luo, X.-L.; Kubas, G. J.; Burns, C. J.; Butcher, R. J.; Bryan, J. C. *Inorg. Chem.* **1995**, *34*, 6538. Ditungsten μ-dinitrogen complexes: (bb) Anderson, S. N.; Richards, R. L.; Hughes, D. L. *J. Chem. Soc., Chem. Commun.* **1982**, 1291. (cc) Anderson, S. N.; Richards, R. L.; Hughes, D. L. *J. Chem. Soc., Dalton Trans.* **1986**, 245. (dd) Churchill, M. R.; Li, Y.-J.; Theopold, K. H.; Schrock, R. R. *Inorg. Chem.* **1984**, *23*, 4472. (ee) Murray, R. C.; Schrock, R. R. *J. Am. Chem. Soc.* **1985**, *107*, 4557. (ff) Churchill, M. R.; Li, Y.-J. *J. Organomet. Chem.* **1986**, *301*, 49. (gg) O'Regan, M. B.; Liu, A. H.; Finch, W. C.; Schrock, R. R.; Davis, W. M. *J. Am. Chem. Soc.* **1990**, *112*, 4331. (hh) Harlan, C. J.; Jones, R. A.; Koschmieder, S. U.; Nunn, C. M. *Polyhedron* **1990**, *9*, 669. Dimanganese and ditechnetium μ-dinitrogen

complexes: (ii) Weidenhammer, K.; Herrmann, W. A.; Ziegler, M. L. *Z. Anorg. Allg. Chem.* **1979**, *457*, 183. (jj) Joachim, J. E.; Apostolidis, C.; Kanellakopulos, B.; Maier, R.; Meyer, D.; Rebizant, J.; Ziegler, M. L. *J. Organomet. Chem.* **1993**, *455*, 137.

4. (a) Laplaza, C. E.; Cummins, C. C. Science 1995, 269, 861. (b) Laplaza, C. E.; Johnson, M. J. A.; Peters, J. C.; Odom, A. L.; Kim, E.; Cummins, C. C.; George, G. N.; Pickering, I. J. *J. Am. Chem. Soc.* **1996**, *118*, 8623.

5. Dinuclear μ-dinitrogen complexes of iron, ruthenium, or osmium: (a) Berke, H.; Bankhardt, W.; Huttner, G.; von Seyerl, J.; Zsolnai, L. *Chem. Ber.* **1981**, *114*, 2754. (b) Che, C.-M.; Lam, H.-W.; Tong, W.-F.; Lai, T.-F.; Lau, T.-C. *J. Chem. Soc., Chem. Commun.* **1989**, 1883. (d) Sellmann, D.; Friedrich, H.; Knoch, F.; Moll, M. *Z. Naturforsch.* **1994**, *49b*, 76. Dinuclear μ-dinitrogen complexes of cobalt, rhodium, or iridium: (d) Cecconi, F.; Ghilardi, C. A.; Midollini, S.; Moneti, S.; Orlandini, A.; Bacci, M. *J. Chem.Soc., Chem. Commun.* **1985**, 731. (e) Klein, H.-F.; Beck, H.; Hammerschmitt, B.; Koch, U.; Koppert, S.; Cordier, G. *Z. Naturforsch.* **1991**, *B46*, 147. (f) Yoshida, T.; Okano, T.; Thorn, D. L.; Tulip, T. H.; Otsuka, S.; Ibers, J. A. *J. Organomet. Chem.* **1979**, *181*, 183. (g) Gutie´rrez, E.; Monge, A.; Nicasio, M. C.; Poveda, M. L.; Carmona, E. *J. Am. Chem. Soc.* **1994**, *116*, 791. Dinickel μ-dinitrogen complexes: (h) Jolly, P. W.; Jonas, K.; Kruger, C.; Tsay, Y.-H. *J. Organomet. Chem.* **1971**, *33*, 109.

6. (a) Che, C.-M, Lam, H.-W.; Tong, W.-F.; Lai, T.-F.; Lau, T. C. *J. Chem. Soc.; Chem. Commun.* **1989**, 1883. (b) Magnuson, R. H.; Taube, H. *J. Am. Chem. Soc.* **1972**, *94*, 7213. (c) Demadis, K. D.; Meyer, T. J.; White, P. S. *Inorg. Chem.* **1997**, *36*, 5678. (d) Leigh, G.

J. *Science* **1995**, *268*, 827. (e) Tuczek, F.; Lehnert, N. *Angew. Chem., Int. Ed. Engl.* **1998**, *37*, 2636. (f) Fryzuk, M. D.; Johnson, S. A. *Coord. Chem. Rev.* **2000**, *200-202*, 379.

7. Smith, J. M.; Lachicotte, R. J.; Pittard, K. A.; Cundari, T. R.; Lukat-Rodgers, G.; Rodgers, K. R.; Holland, P. L. *J. Am. Chem. Soc.* **2001**, *123*, 9222.

8. (a) Betley, T. A.; Peters, J. C. *J. Am. Chem. Soc.* **2003**, *125*, 10782. (b) Betley, T. A.; Peters, J. C. *J. Am. Chem. Soc.* **2004**, *126*, 6252.

9. Betley, T. A.; Peters, J. C. *Inorg. Chem.* **2003**, *42*, 5074.

10. Detrich, J. L.; Konecny, R.; Vetter, W. M.; Doren, D.; Rheingold, A. L.; Theopold, K. H. J. Am. Chem. Soc. 1996, 118, 1703.

11. Brown, S. D.; Peters, J. C. *J. Am. Chem. Soc.* **2005**, *127*, 1913.

12. SQUID magnetization data will be collected shortly on the Co^{I}—N_2—Co^{I} complex $([PhBP^{iPr}_3]Co)_2(\mu\text{-}N_2)$ (**3.8**), though the magnetic moment (5.25 B.M.) via the method of Evans suggests the complex is also ferromagnetically coupled.

13. Kahn, O. *Molecular Magnetism*; VCH Publishers: New York, 1993; pp 1-10.